Stochastic models of partial discharge activity in solid and liquid dielectrics

A.L. Kupershtokh, D.I. Karpov, D.A. Medvedev, C.P. Stamatelatos, V.P. Charalambakos, E.C. Pyrgioti and D.P. Agoris

Abstract: A new model that can reproduce main stochastic features of partial discharge (PD) activity at AC and DC voltages was proposed. The type of PD activity because of microdischarges in small cavities present in dielectric materials was considered. Three different criteria were used to simulate an initiation of partial discharge inside voids. The simplest criterion of threshold type was used also to describe a decay of plasma in voids and subsequent decrease in conductivity to zero. After AC voltage was applied to solid dielectric, the narrow peaks of current in external circuit were observed in our simulations. Every peak corresponds to a moment of PD in a void. The behaviour of cavities in dielectric liquid under DC voltage was also simulated. In this case, PD activity is possible even under DC voltage because of both elongation of microbubbles present in a liquid and diffusion of charge carriers from the surface of a bubble into a liquid.

1 Introduction

One should distinguish three main types of partial discharge (PD) activity [1–3]. The first type of PD activity is the discharges in small cavities existing on surfaces of electrodes and in bulk of dielectric materials. Each individual partial discharge will be called 'microdischarge' where it is more appropriate. The second type is the PD along the surface between two different dielectrics (usually condensed dielectric – gas). The third type is the partial discharges in channels of growing trees. The second and third types of PD can be considered as incomplete breakdown because the insulation properties of dielectric are violated in both cases. Numerous experimental investigations of all types of PD were made. The most full information on PD is in so-called phase resolved data. The series of works are devoted to simulation of PD activity of third type [4–7].

We considered only the PD activity of the first type that occurs at comparatively low voltage here. Small gas-filled cavities existing in solid and liquid dielectrics can influence the electric strength and the lifetime of equipment. The local electric field rather than the average applied field controls the inception of microdischarges in cavities. The gas inside cavities has much lower electric strength than liquid or solid dielectrics. Moreover, if there are no free electric charges on a void walls, electric field magnitude inside cavities is higher than outside in accordance with the permittivity ε of a liquid or a solid. Since some interval after microdischarge, the discharge extinguishes because of decrease in electric field in a void because of accumulation of electric charges near the surface of a void.

Often, the Whitehead's equivalent circuit modelling approach (based on lumped capacitances) is used to study the behaviour of embedded cavities in solid dielectrics [8–10].

The PD activity has essentially stochastic nature. Stochastic features of PDs manifest themselves in variations of time of initiation of PD events (consequently, the time intervals between PDs) and of magnitude of current peaks. Hence, the appropriate methods should be used to simulate this process. In [9], one of the first Monte Carlo simulations of PD activity based on the Whitehead's equivalent circuit model of void was carried out. The probability of PD events was assumed to be proportional to the overvoltage. Only few attempts to take into account the essentially stochastic nature of PD events in simulations were made later in [11–15]. Nevertheless, in these works, the evolution of distribution of electric field in time and space was not taken into account. Hence, all these models are insensitive to a position of the voids and bubbles in gap space and cannot take into account the possible effect of a microdischarge in one cavity onto other cavities.

In [16], the electric-field distribution was calculated directly for single disc-void using Poisson's equation. It was assumed that a microdischarge inside large enough void does not fill the whole volume of the void but rather consists of branched streamer channels. The last circumstance was confirmed experimentally in [17]. For flat voids about 1 mm thick and 40 mm in diameter, the pattern of discharge consisted of hundreds of bright spots distributed uniformly over the cross section of the void. Characteristic diameter of a single spot was of order of 1 mm.

The detailed PD structure was studied in [18]. Each PD was revealed to be a complex conducting structure in a cavity. Conducting channel was observed between the two opposite surfaces of a cavity. Branching creeping discharge developed from both ends of channel along the surfaces. The characteristic size of each creeping discharge was about the same as the gap between the opposite surfaces of a cavity. The patterns of the conducting channels are more complex for the cavities with the gap lengths larger than 1 mm.

IET Sci. Meas. Technol., 2007, **1**, (6), pp. 303–311

303

Hence, in the present work, we propose a new model that can reproduce main stochastic features of partial discharge activity at AC and DC voltage for system of small compact voids of characteristic size less than 1 mm. The first objective of our paper is to take into account correctly the evolution of electric field distribution in time in dielectric material with voids that allows us to study the mutual interaction between neighbour cavities. The second objective is to include more general local stochastic criteria of microdischarge inception inside voids into model of PD. The third objective is also to describe the effect of hydrodynamic flows in liquid dielectric (resulting in deformation and elongation of bubbles in electric field) on PD activity.

PD activity in voids (in solid dielectric) and in bubbles (in a liquid) under AC voltage is similar because of the same physics of gas discharge involved. The main difference is elongation of bubbles in time because of hydrodynamic flows. Moreover, we took into account the diffusion of electric charge carriers from the surface of the bubble into liquid. Therefore, the phase resolved data of PD in solid dielectric can differ insignificantly from the phase resolved data of PD in liquids at least until the influence of chemical decomposition and surface erosion in the voids is small. At the same time, the PD activity in dielectric liquid is possible even under DC voltage.

As our simulations at this stage of investigation are mainly qualitative, we used the arbitrary (dimensionless) units for all parameters and variables (time, space, density, conductivity, surface tension, electric field, and so on). Quantitative calculations could be possible provided that the evolution of plasma channels in gas-filled voids is accurately described. It is practically impossible at present mainly because of the complex physics of gas discharge.

2 Model of partial discharges in solid dielectrics

We used three criteria of microdischarge inception in a void here. The simplest criterion is the well-known field threshold criterion (FTC) $E > E_*$, where E is the local electric field strength, E_* is the threshold field for PD initiation. This criterion is completely deterministic.

It is well known that nonlinear equations exhibit a chaotic behaviour at some region of parameters. From the physical point of view, it means as a rule that the system is in thermodynamically unstable state. Obviously, the state of a dielectric stressed by high electric field is unstable before breakdown. So, the equations of electrodynamics and material equations (that give non-linear positive feed-back) have solutions showing deterministic chaos. Several attempts to bring to light this fact were made in [19, 20].

Unfortunately, the exact equations of breakdown in solid and liquid dielectrics are unknown. Moreover, it should be noted that microprocesses taking place in a material (such as ionisation, recombination, electron avalanche inception) are essentially stochastic and should be described by the laws of quantum mechanics and statistical physics. Moreover, each dielectric has local fluctuations of structure and compositions that are purely random. So, the question about the roles of stochastic and deterministic processes is opened.

We consider here that the stochasticity appears mainly because the discharge begins from primary electrons appearing randomly in a gas that can lead to avalanching. The electron appearance is a rare event with exponential distribution. To describe the stochastic nature of partial discharge inception inside cavities, we used two stochastic criteria. The first one is the field fluctuation criterion (FFC) that was applied earlier in [21–23] to describe growth and

branching of streamer channels. If the condition

$$E > E_* - \delta \qquad (1)$$

was fulfilled in a cavity, then the microdischarge occurred in this cavity at this time step τ. An exponential probability distribution for fluctuation δ was used

$$\varphi(\delta) = \frac{\exp(-\delta/g)}{g} \qquad (2)$$

which is equivalent to the choice of a random value $\delta = -g\ln(\xi)$. Hereafter, ξ is a random number uniformly distributed in the interval from 0 to 1. Parameters E_* and g describe the characteristic electric strength of gas inside a void. In general case, the parameters E_* and g depend on size of cavity and on gas pressure inside it.

The second stochastic criterion is the so-called multi-element stochastic time lag (MESTL) criterion [22, 23]. This criterion was proposed for streamer growth, but actually it defines the stochastic time lag of random events (inception of microdischarges) with exponential distribution function. Hence, it can be applicable also for PD. For all cavities that were in non-conductive state, the stochastic time lags of microdischarge inception

$$\Delta t_i = \frac{-\ln(\xi_i)}{r(E_i)} \qquad (3)$$

were calculated, where i is the number of a cavity. The function $r(E)$ is the reciprocal mean time lag of PD initiation at a local electric field E. This function depends on local electric field inside a cavity and should be sharp enough to describe qualitatively a quasi-threshold character of microdischarges. In general case, this function depends on the size of a cavity and on gas pressure inside it. During one time step τ, the microdischarges occurred in all cavities for which $\Delta t_i < \tau$.

Several different patterns of possible conductive structures arising at PD in a cavity that we used in simulations are shown in Fig. 1, $a-c$. Cavity sizes were 2×2. Only the duration and correspondingly amplitude of each current pulse were different for these patterns. The other results were the same. Nevertheless, the pattern shown in the Fig. 1c. corresponds better to the experimental observations [18]. We assumed that the conductivity of the elements of the conductive structures was equal to a constant value σ_0 during the period of microdischarge.

Several dissipative processes in the plasma of microdischarge (radiation, expansion of plasma channels, and so on) lead to decay of plasma. At present, it is difficult to describe these phenomena exactly. Hence, we used the simplest model based on residual electric field. If the electric field inside the cavity became lower than certain critical value E_{cr} (residual electric field), then we assumed that the microdischarge was extinguished and conductivity became equal to zero (this implies complete decay of
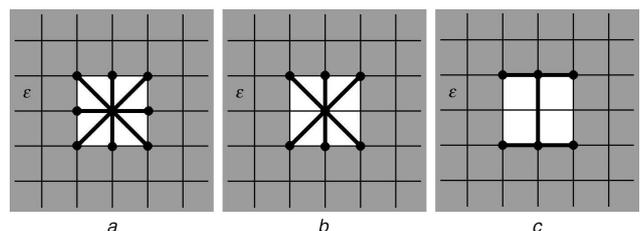

Fig. 1 *Patterns of possible conductive structures arising at PD in a cavity that we used in simulations*

304

IET Sci. Meas. Technol., Vol. 1, No. 6, November 2007

plasma inside cavity because of the reduction of the energy input in comparison with energy loss). Thus, the model proposed describes qualitatively the pulse conductivity inside voids.

To obtain the distributions of the electric-field potential φ and, correspondingly, the electric field $\boldsymbol{E}$ in the region between electrodes, the Poisson's equation

$$\mathrm{div}(\varepsilon\nabla\varphi) = -4\pi q \qquad (4)$$

was solved at each time step together with the equations of conductive transport of charge

$$\frac{\partial q}{\partial t} = -\mathrm{div}\,\boldsymbol{j}, \quad \boldsymbol{j} = \sigma\cdot\boldsymbol{E}, \quad \boldsymbol{E} = -\nabla\varphi \qquad (5)$$

Here ε is the electric permittivity, q is the electric charge density. We supposed that the nonzero conductivity σ and the current density $\boldsymbol{j}$ exist only inside the cavities ($\sigma = 0$ in dielectric outside cavities).

The problem was solved in a two-dimensional rectangular domain. The electric field potential φ was set equal to zero at the surface of lower electrode and equal to applied voltage V at the surface of upper electrode. The periodic boundary conditions were used in x direction.

The transport of electric charge because of conductivity was calculated in parallel with solving the Poisson equation. The time-implicit finite-difference equation for charge transport

$$q^{n+1} = q^n + \tau\,\mathrm{div}(\sigma\nabla\varphi^{n+1}) \qquad (6)$$

was substituted into the finite difference approximation of the Poisson's equation (4), as in [22]. Here n is the number of time step. As a result we have equation

$$\mathrm{div}(\varepsilon\nabla\varphi^{n+1}) = -4\pi(q^n + \tau\,\mathrm{div}(\sigma\nabla\varphi^{n+1})) \qquad (7)$$

that was solved by the method of iterations for values $\varphi^{n+1}_{i,j}$ at every node at the next time step. Then new values of charge density were calculated at every node using (6). This finite-difference scheme ensures exact charge conservation and it is more stable than explicit one.

The system consisted of a set of cavities distributed randomly in a bulk of solid dielectric between plane electrodes was studied (Fig. 2). The dielectric was stressed by AC
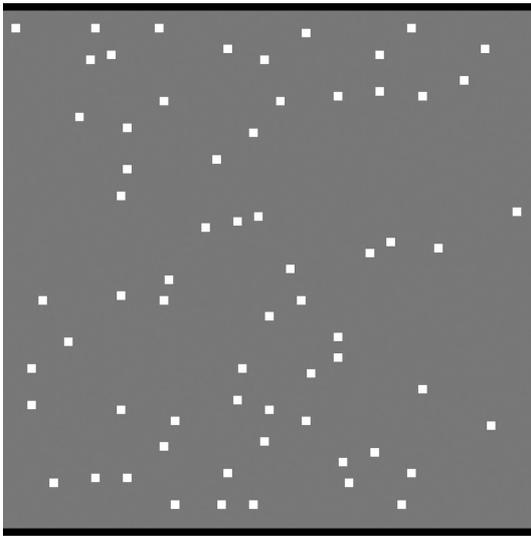

Fig. 2 *Example of a set of cavities randomly distributed in the solid dielectric*

Lattice size 100×100. $N = 65$

voltage $V = V_0\sin(2\pi ft)$ with the amplitude which was high enough for the inception of partial discharges. The time sequence of all microdischarges in cavities, their localisation in the gap and the current in external circuit were registered.

3 Model of partial discharges in dielectric liquid

One of the key stages for breakdown in dielectric liquids is preliminary microdischarges in gas-filled bubbles that are located mainly at the electrode surface (bubble mechanism of breakdown inception). This was confirmed doubtlessly by the experiments on breakdown in water with penetrable porous electrodes (so-called 'diffusive' electrodes) [24] that provided the thin layers of electrolyte near the surfaces of electrodes. In these conductive layers, the electric field was negligible and the microbubbles that are always present at the surface are screened. As a result, the effective impulse electric strength of water increased by a factor of four.

To simulate the partial discharges in liquids, it is necessary to take into account the hydrodynamic flows of fluid in the vicinity of cavities because of their deformation under the action of electric field. To simulate the microdischarges inception in bubbles, we used two criteria described above. The first one was the deterministic criterion FTC. The second one was the stochastic criterion FFC.

3.1 System of electrohydrodynamic equations

Hydrodynamic equations are the continuity equation

$$\frac{\partial\rho}{\partial t} + \nabla(\rho\boldsymbol{u}) = 0 \qquad (8)$$

and the Navier–Stokes equation

$$\frac{\partial\rho\boldsymbol{u}}{\partial t} + \nabla\Pi^{(0)}_{\alpha\beta} = \boldsymbol{F} + \eta\nabla^2\boldsymbol{u} + \left(\zeta + \frac{\eta}{3}\right)\mathrm{grad\,div}\,\boldsymbol{u} \qquad (9)$$

Here ρ is the density of liquid, $\boldsymbol{u}$ is the velocity of fluid flow, $\boldsymbol{F}$ is the body force, $\Pi^{(0)}_{\alpha\beta} = p\delta_{\alpha\beta} + \rho u_\alpha u_\beta$ is the non-viscous part of the momentum flux tensor, p is the pressure, η and ζ are the dynamic and second viscosities and $\delta_{\alpha\beta}$ is the Kronecker delta.

Equations for concentrations n_i of electric charge carriers are

$$\frac{\partial n_i}{\partial t} + \nabla(n_i\boldsymbol{u}) = D_i\Delta n_i - \mathrm{div}\left(\frac{q_i}{|q_i|}b_i n_i\boldsymbol{E}\right) + w_i - r_i \qquad (10)$$

Here D_i are the diffusivities, b_i are the macroscopic effective mobilities of charge carriers q_i; w_i and r_i are the rates of ionisation and recombination of charge carriers (they were neglected in bulk of dielectric in this work).

The Poisson's equation for potential of electric field φ is

$$\mathrm{div}(\varepsilon\nabla\varphi) = -4\pi q, \quad \boldsymbol{E} = -\nabla\varphi \qquad (11)$$

Here $q = \sum_i q_i n_i$ is the total electric charge density.

The electric force acting on elementary volume in liquid is

$$\boldsymbol{F} = q\boldsymbol{E} - \frac{E^2}{8\pi}\nabla\varepsilon + \frac{1}{8\pi}\nabla\left(E^2\rho\frac{\partial\varepsilon}{\partial\rho}\right) \qquad (12)$$

where the last term is the electrostriction force that cannot be considered as small.

The electric current can be expressed as

$$\boldsymbol{j} = \sum_i (q_i n_i \boldsymbol{u} - D_i q_i \nabla n_i + b_i |q_i| n_i \boldsymbol{E})$$

$$= q\boldsymbol{u} - \sum_i D_i q_i \nabla n_i + \sigma \boldsymbol{E} \qquad (13)$$

The local conductivity $\sigma = \sum_i b_i |q_i| n_i$ depends on local concentrations of charge carriers and can vary in space and in time.

In the case of constant and equal diffusion coefficients $D_i = D$, multiplying (10) by q_i and summing over all i, we obtain the equation for total charge density q

$$\frac{\partial q}{\partial t} + \nabla(q\boldsymbol{u}) = D\Delta q - \mathrm{div}(\sigma \boldsymbol{E}) \qquad (14)$$

that can be used instead of the set of equations (10).

In our calculations, the value of conductivity σ was assumed to be constant for simplicity.

3.2 Method of splitting

To solve the system of equations (8), (9), (11), (12) and (14), the method of splitting in physical processes [25] was used. The whole time step was divided into several stages implemented sequentially. These stages were as follows.

1. Modelling of hydrodynamic flows.
2. Simulation of convective transport and diffusion of charge carriers [(14) without the last term].
3. Calculation of electric potential and charge transfer because of mobility of charge carriers (conductivity).
4. Calculation of electrostatic forces acting on elementary volume in liquid.
5. Simulation of phase transition.
6. Simulation of partial discharges inside cavities.

The lattice Boltzmann equation (LBE) method was used to simulate the hydrodynamic flows and also the convective transport and diffusion of charge carriers [26, 27]. The exact difference method (EDM) [27–29] was used to take into account the body force term in the LBE method. Evolution of potential distribution, charge transport because of mobility of charge carriers and components of electric forces were calculated by finite-difference method.

3.3 Simulation of phase transition in LBE method

In LBE methods, different phases are simulated uniformly. Hence, there is no need in an explicit interface tracking. Boundaries between liquid and gas are represented as thin transition layers of finite width (several lattice nodes) where density changes smoothly from one bulk value to another. Hence, the possible topological changes of interface boundaries (generation, disappearance, reconnections) are simulated without any interface tracking.

To simulate these transition layers, the special mesoscopic forces were introduced in LBE model [30, 31] that act between every pair of neighbour nodes. The sum of these forces that act on the matter in the node is equal to

$$\boldsymbol{F}_{\mathrm{N}}(\boldsymbol{x}) = \psi(\rho(\boldsymbol{x})) \sum_k G_k \psi(\rho(\boldsymbol{x} + \boldsymbol{e}_k)) \boldsymbol{e}_k \qquad (15)$$

Here G_K are the coefficients different for basic and diagonal directions, $\psi(\rho)$ is an increasing function of density. These forces are attractive at $G_k > 0$. For this model, the equation

of state has the form

$$p = \rho\theta - \alpha G_0 \psi^2 \qquad (16)$$

where G_0 is the coefficient in (15) corresponding to basic directions of the lattice. Here $\theta = kT/m$ is the reduced temperature. In the series of isothermal LBE models [32]: one-dimensional model D1Q3, two-dimensional model D2Q9 and three-dimensional model D3Q19, the appropriate reduced temperature is $\theta = (h/\Delta t)^2/3$. The coefficients for diagonal directions G_1 that ensure the isotropy of space are equal to 0, $G_0/4$ and $G_0/2$ for these three models, and the corresponding coefficients α are equal to 1, 3/2 and 3, respectively.

For certain form of function $\psi(\rho)$, the equation of state (16) allows a phase transition for this isothermal model. Particularly, the phase transition exists for the function proposed in [30, 31]

$$\psi(\rho) = \rho_0(1 - \exp(-\rho/\rho_0)) \qquad (17)$$

The critical point corresponds to $G_{0*} = 2\theta/(\alpha\rho_0)$ and $\rho_* = \rho_0 \ln 2$. In one-dimensional case at $\rho_0 = 1$ we have $\rho_* = 0.693$ and $G_{0*} = 2/3$. For the values of $G_0 > G_{0*}$, coexistence of dense (liquid) and rarefied (gaseous) phases is possible. In this case, the forces (15) ensure the surface tension of liquid–gas interface. The value of surface tension λ depends on the value of parameter G_0 [31].

To simulate the phase transitions for other form of equation of state $p(\rho, T)$, Zhang and Chen [33] introduced a special force acting on the matter in every node. This force should be a gradient of certain potential U (mean-field approach) to ensure the global momentum conservation law (if external forces are absent)

$$\boldsymbol{F}_{\mathrm{N}} = -\nabla U \qquad (18)$$

Zhang and Chen proposed to express this potential using the equation of state as

$$U = p(\rho, T) - \rho\theta \qquad (19)$$

In [33], the finite-difference approximation of (18) was proposed $\boldsymbol{F}_{\mathrm{N}} = \sum_k b_k U(\boldsymbol{x} + \boldsymbol{e}_k)\boldsymbol{e}_k$, where coefficients b_k were found only for simplest D2Q7 model with equal vectors of particle velocity.

In the framework of isothermal LBE models [30, 31], the following formula for function $\psi(\rho)$ was obtained in [34, 35]

$$\psi(\rho) = \sqrt{\frac{-(p(\rho) - \rho\theta)}{(\alpha G_0)}} \qquad (20)$$

for equations of state in the form $p(\rho)$.

We proposed to use a function

$$\Phi = \sqrt{-U} \qquad (21)$$

that is similar to (20) also for Zhang and Chen model (18) and (19). Then, for one-dimensional case (D1Q3), the finite-difference approximation of (18) can be written in the form

$$F_i = -\frac{U_{i+1} - U_{i-1}}{2h} = \frac{(\Phi_{i+1} + \Phi_{i-1})}{2} \frac{(\Phi_{i+1} - \Phi_{i-1})}{h} \qquad (22)$$

At the same time, one can obtain new expression

$$\boldsymbol{F}_{\mathrm{N}} = 2\Phi(\rho, T)\nabla\Phi(\rho, T) \qquad (23)$$

considering the force $\boldsymbol{F}_{\mathrm{N}}$ (18) acting on the matter in the node. We proposed to represent the finite-difference

approximation of this vector in the form

$$\boldsymbol{F}_\mathrm{N} = \frac{1}{\alpha h}\Phi(\boldsymbol{x})\sum_k \frac{G_k}{G_0}\Phi(\boldsymbol{x}+\boldsymbol{e}_k)\boldsymbol{e}_k \qquad (24)$$

If we define $\Phi(\rho) = \sqrt{\alpha G_0}\,\psi(\rho)$ and $h = 1$ (as usually is assumed in LBE method), the form of force approximation (24) is equivalent to (4) that was used for isothermal LBE method [30, 31].

Hence, in one-dimensional case ($\alpha = 1$, $G_k = G_0$), we have another finite-difference approximation for (18)

$$F_i = \Phi_i\frac{(\Phi_{i+1} - \Phi_{i-1})}{h} \qquad (25)$$

that is different from (22). Namely, the local value of function Φ_i in the given node is used in (25) instead of the average value $\bar{\Phi} = (\Phi_{i-1} + \Phi_{i+1})/2$ in (22).

For the van der Waals equation of state in reduced variables $\tilde{p} = p/p_\mathrm{cr}$, $\tilde{\rho} = \rho/\rho_\mathrm{cr}$, $\tilde{T} = T/T_\mathrm{cr}$

$$\tilde{p} = \frac{8\tilde{T}\tilde{\rho}}{3 - \tilde{\rho}} - 3\tilde{\rho}^2 \qquad (26)$$

the theoretical coexistence curve was calculated using the Maxwell rule (Fig. 3, curve 1). Here p_cr, ρ_cr, and T_cr are the critical values of liquid–vapour transition. If one exploits the system of these reduced units in the LBE method, one should use the coefficient $k = p_\mathrm{cr}/\rho_\mathrm{cr}(\Delta t/h)^2$ (it depends on the values of pressure and density in critical point for a specific dielectrics) to substitute a pressure in reduced units into LBEs.

The simulation results agree well with the theoretical values of liquid density at the coexistence curve. However, it turned out that the values for vapour density depend strongly on the variant of approximation of forces (22) or (25) used. The simulation results are very inaccurate for both these approximations in the range of comparatively low temperatures. Nevertheless, the approximation (25) gives the results (Fig. 3, curve 2) that agree much better with the theoretical ones than the results (Fig. 3, curve 3) obtained using the approximation (22).

To improve the method, we proposed new more general finite-difference approximation of (18) and (21) in the form of linear combination of (22) and (25) with some coefficient A

$$F_i = [A\Phi_{i+1} + (1 - 2A)\Phi_i + A\Phi_{i-1}]\frac{(\Phi_{i+1} - \Phi_{i-1})}{h} \quad (27)$$
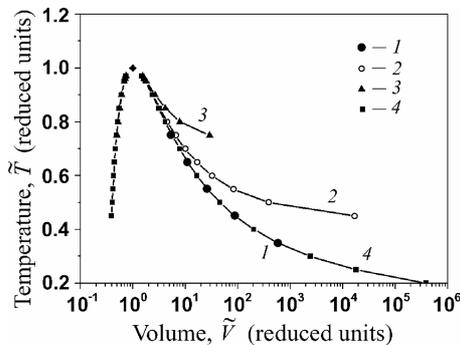

Fig. 3 *Coexistence curve for van der Waals equation of state*
Curve 1 is the theoretical coexistence curve, curve 2 is the approximation (25), curve 3 is the approximation (22), and curve 4 is the approximation (27)

This formula is applicable for model (18), (21) that allows to exploit an arbitrary form of equation of state $p(\rho, T)$ using (19).

The deviations of results obtained using the approximation (27) (Fig. 3, curve 4) from the theoretical values are less then 0.4% at $A = -0.152$ in the range from the critical point $\tilde{T} = 1$ down to $\tilde{T} = 0.4$. The EDM [27–29] was used to include the body force term in LBE method for all these variants of approximations.

For two-dimensional LBE model D2Q9 and for three-dimensional LBE model D3Q19, we proposed the following approximation that in vector form is

$$\boldsymbol{F}_\mathrm{N}(\boldsymbol{x}) = \frac{1}{\alpha h}\Bigg[(1 - 2A)\Phi(\boldsymbol{x})\sum_k \frac{G_k}{G_0}\Phi(\boldsymbol{x}+\boldsymbol{e}_k)\boldsymbol{e}_k$$
$$+ A\sum_k \frac{G_k}{G_0}\Phi^2(\boldsymbol{x}+\boldsymbol{e}_k)\boldsymbol{e}_k\Bigg] \qquad (28)$$

The coefficients $G_k = 1/4$ for diagonal directions of approximation in (28) can be obtained considering the projection of all forces that act between nodes of four-dimensional face-centered hypercubic lattice in the LBE model D4Q25 onto the square lattice in two-dimensional space. The model D4Q25 obviously has enough isotropy [36]. In this model, 24 vectors of forces act on the node in four-dimensional space. The absolute values of all these forces are equal and proportional to $G_0\sqrt{2}$ for locally uniform state of matter.

For model D2Q9, the finite-difference approximation of the x component of force acting on the node F_N has the following form

$$(F_{i,j})_x = \frac{2}{3h}$$
$$\times\Bigg\{(A\Phi_{i+1,j} + (1 - 2A)\Phi_{i,j} + A\Phi_{i-1,j})(\Phi_{i+1,j} - \Phi_{i-1,j})$$
$$+ \frac{1}{4}\Big[(A\Phi_{i+1,j+1} + (1 - 2A)\Phi_{i,j} + A\Phi_{i-1,j-1})$$
$$\times(\Phi_{i+1,j+1} - \Phi_{i-1,j-1}) + (A\Phi_{i+1,j-1} + (1 - 2A)\Phi_{i,j}$$
$$+ A\Phi_{i-1,j+1})(\Phi_{i+1,j-1} - \Phi_{i-1,j+1})\Big]\Bigg\} \qquad (29)$$

The similar expression was used for the y component of force. The proposed form of approximation ensures correct coexistence curve and, hence, the values of surface tension and also correct circular shape (in stationary case without external forces) of both droplets in a vapour and bubbles in a liquid.

4 Simulation results

4.1 Partial discharges in solid dielectrics

The system consisted of a set of cavities randomly distributed in a bulk of solid dielectric between two plane electrodes was studied. The dielectric was stressed by AC voltage that was high enough for the inception of partial discharges. The MESTL criterion was used for inception of microdischarges in cavities. The function $r(E) = BE^4$ was used in these simulations. After some interval, the discharge extinguishes because of decrease in electric field in a void because of the accumulation of electric charges near the surface of a void.

Lattice size was 100×100. Hence, distance between electrodes L was equal to 100 lattice units. The parameters

were $f = 50$ Hz, $\varepsilon = 2$, $B = 10^5$, $E_{cr} = 0.1$. Hereafter, we will use the system of arbitrary units for voltage and current.

We registered the electric current in external circuit in our simulations. Narrow peaks were observed at the moment of every microdischarge. Typical plots are shown in Fig. 4. Increase in voltage led to more frequent partial discharges (Fig. 4b). The amplitudes of current peaks also increased. During the first half period of voltage, practically all microdischarges occurred in uncharged voids. Hence, the distribution of peaks against phase is obviously different from distributions at all subsequent half periods. As we used probability distribution for inception of microdischarges in cavities, our simulations of the moments and the amplitudes of PD reflect their stochastic nature. A set of cavities for typical variant of simulations is shown in Fig. 5. Sign (∗) marks those cavities that were conductive at the moment corresponding to the state shown in this figure. Obviously, the corresponding electric current peak was greater in magnitude than usually. The phase resolved data on PD obtained in simulations are in qualitative agreement with experimental results [9]. The frequency and magnitudes of PD increase with voltage that also is in qualitative agreement with experimental results. All the simulations were performed for several sets of parameters. At every set of parameters, simulations were performed several times. Obviously, the results of simulations cannot be repeatable in details because of the stochastic nature of the process. Nevertheless, the averaged characteristics of the process were repeatable quite well.

The behaviour of a single void in electric field was also simulated to clarify the process in detail. The relative electric field inside a single void is shown in Fig. 6a. Before the first microdischarge in the cavity, the electric field inside it was somewhat greater than the current value of undisturbed uniform electric field between electrodes $E = E_0 \sin(2\pi f t)$ because of the value of permittivity of a solid dielectric $\varepsilon > 1$ and the compact shape of the void. Here, $E_0 =$
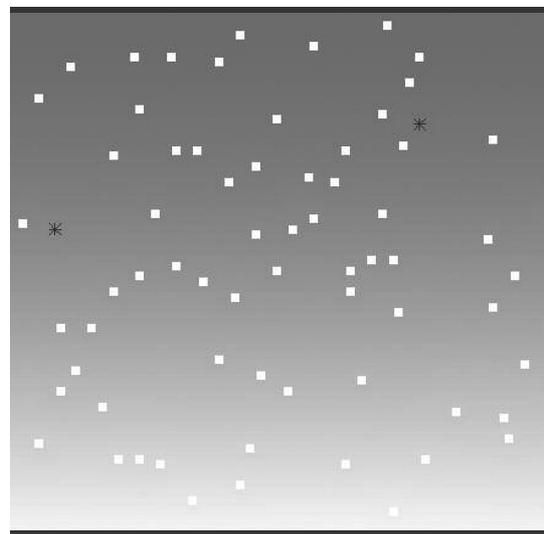

Fig. 5 *Set of cavities for typical variant of simulations*

Potential distribution from $\varphi = 0$ at lower electrode to $\varphi = V_0$ at upper electrode is shown by gray levels. $N = 68$. Lattice size 100×100

V_0/L is the amplitude of electric field in a solid dielectric. For example, the well-known result for internal electric field in spherical uncharged void having diameter much smaller than the length of interelectrode gap is $E_V = 3E\varepsilon/(2\varepsilon + 1)$ [37]. If applied voltage was high enough but remained below breakdown voltage of a solid dielectric, then the partial discharges in void occurred several times per period (Fig. 6a). The values of internal electric field just before every microdischarge varied stochastically in some range in accordance with MESTL criterion. Correspondingly, the amplitudes of peaks of current also changed randomly.

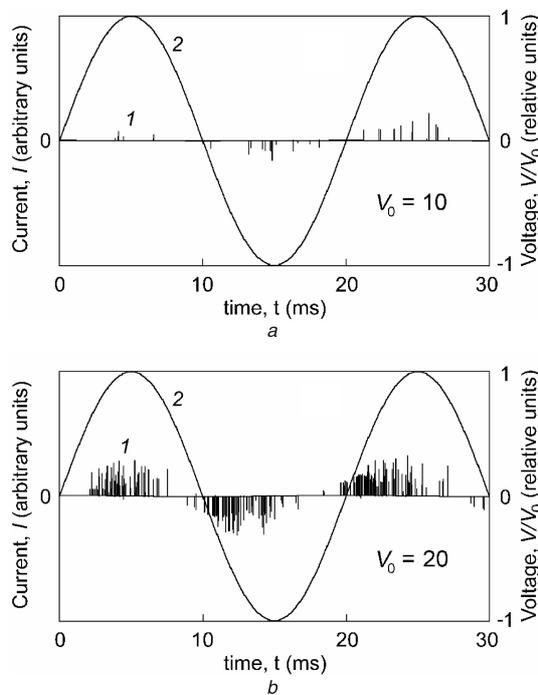The behaviour of coupled (close located) cavities was also simulated. The distance between two coupled voids

Fig. 4 *Partial discharge activity during three half periods of voltage (curves 1)*

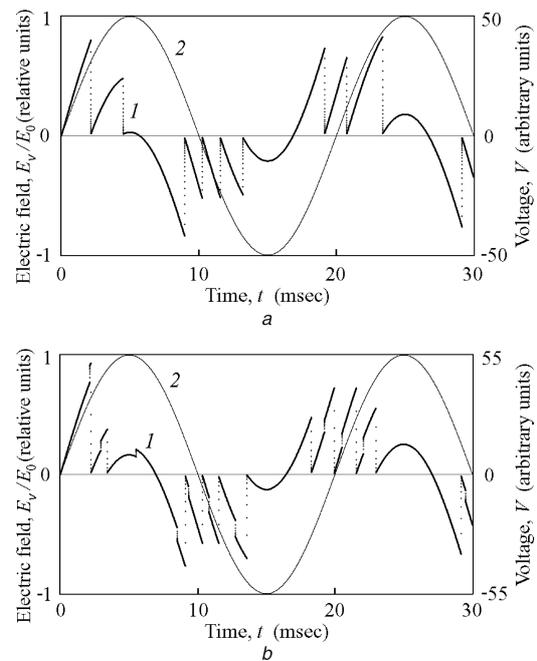Applied voltage (curves 2)
a $V_0 = 10$, $N = 70$
b $V_0 = 20$, $N = 75$

Fig. 6 *Relative electric field inside a void in solid dielectric (curves 1)*

a Single void
b Coupled voids
Applied voltage (curves 2). $\varepsilon = 2$, $V_0 = 50$

was 3 lattice units. The influence of microdischarge in one cavity on probability of inception of microdischarges in neighbour cavities was demonstrated. The change of the relative electric field inside one of the coupled voids (located one close other in the direction along field) is shown in Fig. 6b. It is clearly seen that the internal electric field in one void increased sharply after microdischarge and subsequent polarisation in the neighbour void. Therefore, the periods between microdischarges in the voids shorten in this case as the probability of microdischarge increases with electric field strength.

4.2. PDs in a single vapour cavity embedded in dielectric liquid

The behaviour of a single spherical cavity in dielectric liquid stressed by constant DC voltage was simulated to clarify the process in detail. The electric strength of gases is much lower than that of liquids. For the right part of Pashen's curve, the breakdown voltage of the cavity increases approximately linearly with the product of pressure and cavity size. Hence, electric field strength of breakdown inside cavity decreases with the longitudinal cavity size. Hence, the electric breakdown can occur only if the vapour bubble becomes larger than a certain critical size. During microdischarge, the bubble is conductive, and the charge accumulates near the bubble-liquid interface. Hence, the bubble begins to deform under the action of electric forces. The dynamics of bubble deformation and growth is shown in Fig. 7. In this simulation, we used FTC criterion for microdischarge inception with the parameter $E_* = 0.2$ of arbitrary units. The residual electric field was $E_{cr} = E_*/2$. Lattice size 200×200 was used. Initial radius of spherical bubble was $R_0 = 15$ lattice units.

The distribution of vertical component of electric field inside and outside the vapour bubble at the moment after one of the microdischarges is shown in Fig. 8. Higher values of electric field are near the poles of the bubble. The plots of current in external circuit are shown in Figs. 9 (FTC) and 10a (FFC). We did not show the first impulse of charging current because of the system's capacitance because it is not a partial discharge. The first PD occurred after a very short delay following the application of the voltage.

As expected, for FFC, the magnitudes of the peaks of PD and intervals between them varied stochastically. The magnitude of a peak of current depended on instantaneous value of internal electric field in the cavity before the moment of microdischarge and on size of cavity especially in the direction of the electric field. The variation of electric field strength in the central part of the bubble is shown in Fig.10b. After every microdischarge, the electric field became equal to E_{cr}. Then, the electric field increased
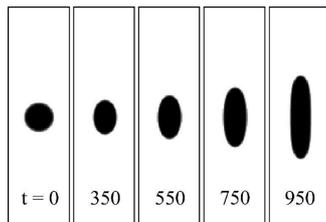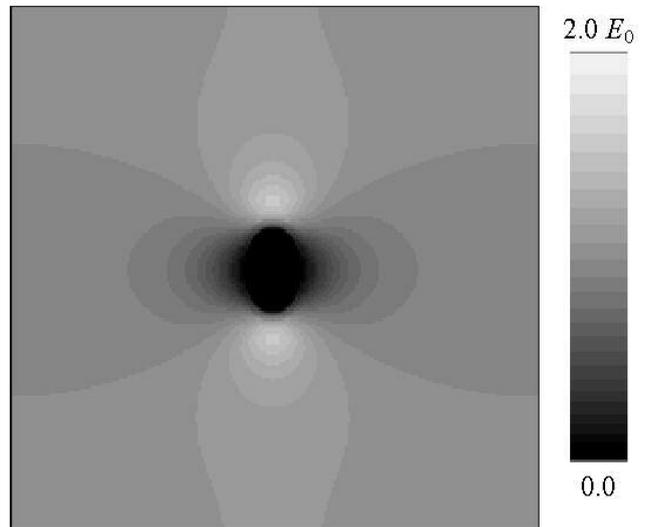

Fig. 8 *Distribution of vertical component of electric field inside and outside vapor bubble at the moment after one of the microdischarges*

Gray levels indicate different values of the vertical component of electric field. Lattice size 200×200. $t = 500$
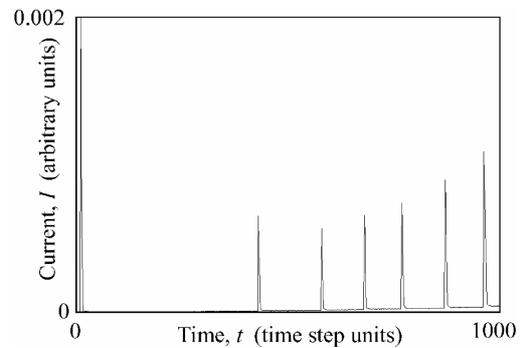

Fig. 9 *Partial discharges in a single vapour bubble embedded in dielectric liquid stressed by constant DC voltage*

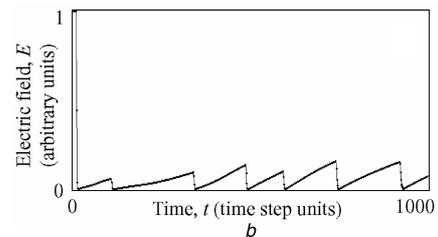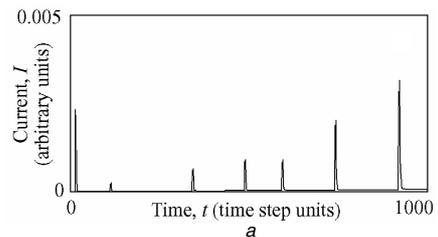LBE model with deterministic criterion for partial discharges (FTC)

Fig. 10 *Partial discharges in a single vapor bubble embedded in dielectric liquid stressed by constant DC voltage*

LBE model with stochastic criterion for partial discharges (FFC)
a Current in external circuit
b Electric field strength in the central part of the bubble
$E_* = 0.2$, $g = 0.1E_*$, $E_{cr} = 0.04E_*$, $V = 200$

Fig. 7 *Behaviour of single spherical vapour cavity in a dielectric liquid stressed by constant DC voltage*

Dark colour corresponds to lower density. Frame size 55×200 lattice units
Hereafter, time will be in time step units

IET Sci. Meas. Technol., Vol. 1, No. 6, November 2007

309

because of the elongation of the bubble and the diffusion of surface charges into liquid. A slowly increasing component of the current existed because of the growth of the polarised bubble (Fig. 7) that carried charges at its surface.

In the case of FTC model, the evolution is obviously purely deterministic (stochasticity is absent absolutely). Every run gave the same results. The electric field strength inside a cavity before each microdischarge is constant E_* in contrast to the results obtained with FFC (Fig. 10b). The different time intervals between microdischarges could be explained by the combined effects of deformation and elongation of bubble under the action of electric forces (12) and charge diffusion.

4.3. Partial discharges in dielectric liquid in vapour cavities located at the electrode surface

Microbubbles always exist in a liquid mostly at the surfaces of electrodes. The series of microdischarges in an initially hemispherical bubble provides charge transfer from the surface of electrode to the pole of this cavity. This leads to the elongation of the cavity under the action of electric field and to a considerable magnification of electric field strength near its top. As a result, the high local electric field can cause the processes in the liquid near the top of this cavity, such as ionisation, which can further lead to the formation of a streamer in a liquid.

Simulations of bubble development with pulse conductivity were performed on a two-dimensional lattice of size 200×200. Microdischarge in a bubble occurred according

to the stochastic FFC model with the parameters $E_* = 1$, $g = 0.008$ and $E_{cr} = 0.0025$ (all in arbitrary units). We considered a dielectric liquid with permittivity close to 1 to investigate clearly a dynamics of free charges (without influence of polarisation charges).

Evolution of bubbles under the action of electric field is shown in Fig. 11. Time was counted from the moment when voltage was applied. Three bubbles of random sizes were randomly placed on lower grounded electrode (Fig. 11a). Shapes of bubbles changed after several microdischarges inside them (Fig. 11d). Fig. 11b shows the distribution of an absolute value of electric field strength at time $t = 473$. The largest values of electric field (light colour) are near the poles of bubbles. Electric charge distribution in interelectrode gap is shown in Fig. 11c for $t = 1328$. Light regions correspond to high densities of negative charge. After each microdischarge in a bubble, a new portion of charge is injected into the bubble from electrode. The charges accumulate near the bubble − liquid interface and diffuse into liquid involving it into the motion.

Fig. 12 shows the electric current in the external circuit. First impulse corresponding to the moment of voltage application is not shown. Every peak corresponds to PD in one of the bubbles. The magnitudes of current pulses corresponding to PD in the bubbles connected electrically with the electrodes (Fig. 12) are significantly larger than for the bubbles located far from electrodes (Figs. 9 and 10a). Continuous component of the current appeared because of the diffusion of free charges in a liquid and elongation of bubbles. The impulses of current that correspond to the
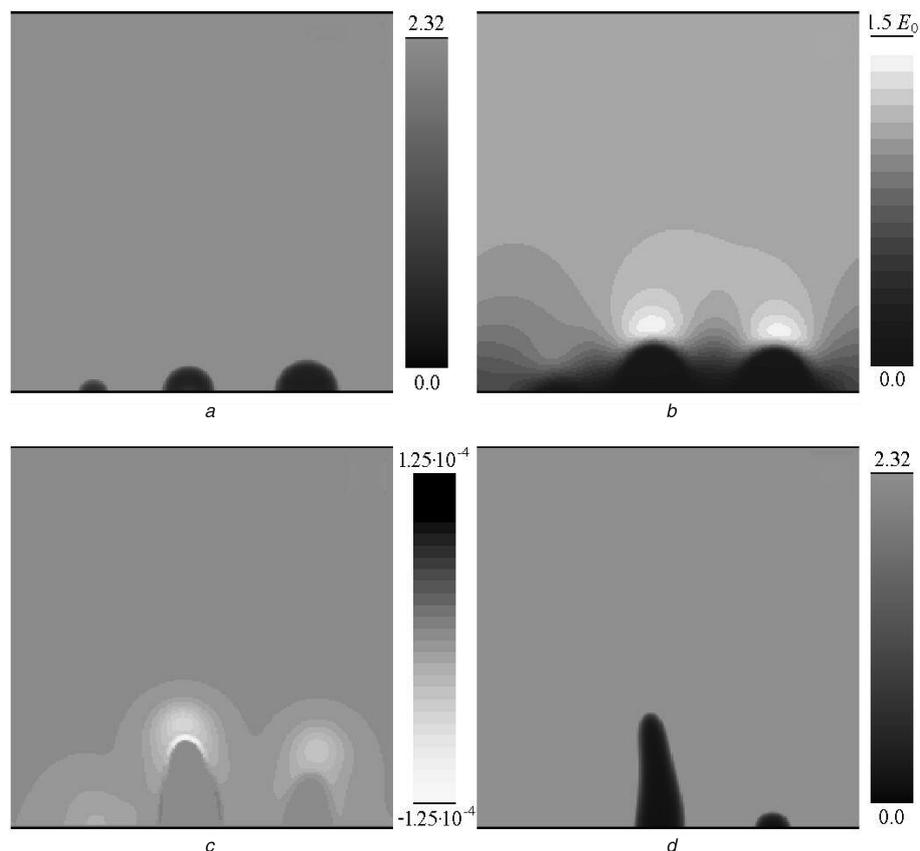

Fig. 11 *Evolution of bubbles located at the surface of electrode*

a Shapes of bubbles at $t = 0$
b Absolute value of electric field strength at $t = 473$
c Distribution of electric charge density at $t = 1328$
d Shapes of bubbles at $t = 1774$
$V = 50$ (arbitrary units). Gray levels correspond to various values of the mass density, charge density and electric field strength. Lattice size 200×200
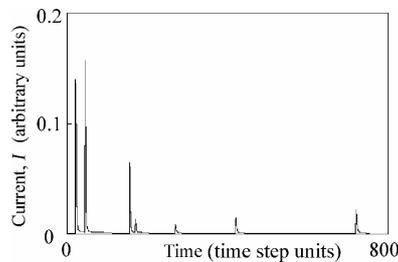
310

IET Sci. Meas. Technol., Vol. 1, No. 6, November 2007

Fig. 12 *Electric current in the external circuit during the period of bubbles development corresponding to* Fig. 11

first PD in every bubble are usually higher than those for subsequent microdischarges.

5 Conclusions

After AC voltage was applied to solid dielectric, the narrow peaks of current in external circuit were observed in our simulations, every peak corresponded to an occurrence of PD in a void. As expected, the magnitudes of the peaks and intervals between them varied stochastically. The PD activity in dielectric liquid is possible even under DC voltage because of both elongation of microbubbles present in a liquid and diffusion of charge carriers from the surface of a bubble into a liquid. The evolution of vapour cavities in dielectric liquid was also simulated in the case when repetitive microdischarges inside cavities occurred.

6 Acknowledgments

7 References

1 Bartnikas, R., and Novak, J.P.: 'On the character of different forms of partial discharge and their related terminologies', *IEEE Trans. Electric, Insul.*, 1993, **28**, pp. 956–968

2 Kreuger, F.H., Gulski, E., and Krivda, A.: 'Classification of partial discharges', *IEEE Trans. Electric. Insul.*, 1993, **28**, pp. 917–931

3 Niemeyer, L.: 'A generalized approach to partial discharge modeling', *IEEE Trans. Dielectrics Electric. Insul.*, 1995, **2**, pp. 510–528

4 Van Brunt, R.J.: 'Stochastic properties of partial discharge phenomena', *IEEE Trans. Electric. Insul.*, 1991, **26**, pp. 902–948

5 Suwarno, Suzuoki, Y., Komori, F., and Mizutani, T.: 'Partial discharges due to electrical treeing in polymers: phase-resolved and time-sequence observation and analysis', *J. Phys. D: Appl. Phys.*, 1996, **29**, pp. 2922–2931

6 Noskov, M.D., Malinovski, A.S., Sack, M., and Schwab, A.J.: 'Self-consistent modeling of electrical tree propagation and PD activity', *IEEE Trans. Dielectrics Electric. Insul.*, 2000, **7**, pp. 725–733

7 Noskov, M.D., Malinovski, A.S., Sack, M., and Schwab, A.J.: 'The simulation of dendrite growth and partial discharges in epoxy resin', *Tech. Phys.*, 2002, **47**, pp. 260–267 (Translated from Russian *Zh. Tekh. Fiz.*, **72**, (2), pp. 121–128

8 Gemant, A., and Von Philipoff, W.: 'Die Funkenstrecke mit Vorkondensator', *Z. Tech. Phys.*, 1932, **13**, pp. 425–430

9 Hikita, M., Yamada, K., Nakamura, A., Mizutani, T., Oohasi, A., and Ieda, M.: 'Measurements of partial discharges by computer and analysis of partial discharge distribution by the Monte Carlo method', *IEEE Trans. Electric. Insul.*, 1990, **25**, pp. 453–468

10 Agoris, D.P., and Hatziargyriou, N.D.: 'Approach to partial discharge development in closely coupled cavities embedded in solid dielectrics by lumped capacitance model', *IEE Proc., A*, 1993, **140**, pp. 131–134

11 Fruth, B., and Niemeyer, L.: 'The importance of statistical characteristics of partial discharge data', *IEEE Trans. Electric. Insul.*, 1992, **27**, pp. 60–69

12 Gutfleish, F., and Niemeyer, L.: 'Measurement and simulation of PD in epoxys voids', *IEEE Trans. Dielectrics and Electric. Insul.*, 1995, **2**, pp. 729–743

13 Heitz, C.: 'A generalized model for partial discharge processes based on a stochastic process approach', *J. Phys. D: Appl. Phys.*, 2001, **32**, pp. 1012–1023

14 Okamoto, T., Kato, T., Yokomizu, Y., and Suzuoki, Y.: 'Fluctuation analysis of partial discharge pulse occurrence with an integral equation', *Electr. Eng. Jpn.*, 2001, **136**, pp. 16–28

15 Cavallini, A., and Montanari, G.C.: 'Effect of supply voltage frequency on testing of insulation system', *IEEE Trans. Dielectrics Electric. Insul.*, 2006, **13**, pp. 111–121

16 Wu, K., Suzuoki, Y., and Dissado, L.A.: 'The contribution of discharge area variation to partial discharge patterns in disk-voids', *J. Phys. D: Appl. Phys.*, 2004, **37**, pp. 1815–1823

17 Morshuls, P.H.F., and Kreuger, F.H.: 'Transition from streamer to Townsend mechanisms in dielectric voids', *J. Phys. D: Appl. Phys.*, 1990, **23**, pp. 1562–1568

18 Zanin, A.L., Liehr, A.W., Moskalenko, A.S., and Purwins, H.-G.: 'Voronoi diagrams in barrier gas discharge', *Appl. Phys. Lett.*, 2002, **81**, pp. 3338–3340

19 Dodd, S.J., Dissado, L.A., Champion, J.V., and Alison, J.M.: 'Evidence for deterministic chaos as the origin of electrical tree breakdown structures in polymeric insulation', *Phys. Rev. B*, 1995, **52**, (24), pp. 16985–16988

20 Dodd, S.J.: 'A deterministic model for the growth of non-conducting electrical tree structures', *J. Phys. D: Appl. Phys.*, 2003, **36**, pp. 129–141

21 Kupershtokh, A.L.: 'Fluctuation model of the breakdown of liquid dielectrics', *Sov. Tech. Phys. Lett.*, 1992, **18**, pp. 647–649. (Translated from Russian *Pis'ma Zh. Tekh. Fiz.*, 1992, **18**, No. 19, pp. 91–96.)

22 Karpov, D.I., and Kupershtokh, A.L.: 'Models of streamer growth with "physical" time and fractal characteristics of streamer structures'. Conf. Record of the 1998 IEEE Int. Symp. Electrical Insulation, Arlington, USA, 1998, IEEE No. 98CH36239, vol. 2, pp. 607–610

23 Kupershtokh, A.L., Charalambakos, V., Agoris, D., and Karpov, D.I.: 'Simulation of breakdown in air using cellular automata with streamer to leader transition', *J. Phys. D: Appl. Phys.*, 2001, **34**, pp. 936–946

24 Vorob'ev, V.V., Kapitonov, V.A., Kruglyakov, E.P., and Tsidulko, Yu.A.: 'Study of breakdown in water using diffusive electrodes', *Zh. Tekh. Fiz*, 1980, **72**, (2), pp. 993–999

25 Yanenko, N.N.: 'The method of fractional steps' (Springer, Berlin, 1967)

26 Kupershtokh, A.L., and Medvedev, D.A.: 'Lattice Boltzmann equation method in electrohydrodynamic problems'. Proc. 5th Int. Workshop on Electrohydrodynamics, Poitiers, France, 2004, pp. 61–65

27 Kupershtokh, A.L.: 'New method of incorporating a body force term into the lattice Boltzmann equation'. Proc. 5th Int. Workshop on Electrohydrodynamics, Poitiers, France, 2004, pp. 241–246

28 Kupershtokh, A.L.: 'Calculations of the action of electric forces in the lattice Boltzmann equation method using the difference of equilibrium distribution functions'. Proc. 7th Int. Conf. Modern Problems of Electrophysics and Electrohydrodynamics of Liquids, St. Petersburg, Russia, 2003, pp. 152–155

29 Kupershtokh, A.L.: 'A body force term in the lattice Boltzmann equation', *Bull. (Quarter Journal)', Novosibirsk State Univ. Ser.: Math. Mech. Inf.*, 2004, **4**, (2), pp. 75–96 [in Russian]

30 Shan, X., and Chen, H.: 'Lattice Boltzmann model for simulating flows with multiple phases and components', *Phys. Rev. E*, 1993, **47**, pp. 1815–1819

31 Shan, X., and Chen, H.: 'Simulation of nonideal gases and liquid-gas phase transitions by the lattice Boltzmann equation', *Phys. Rev. E*, 1994, **49**, pp. 2941–2948

32 Qian, Y.H., and Orzag, S.A.: 'Lattice BGK models for the Navier–Stokes equation: nonlinear deviation in compressible regimes', *Europhys. Lett.*, 1993, **21**, pp. 255–259

33 Zhang, R., and Chen, H.: 'Lattice Boltzmann method for simulations of liquid-vapor thermal flows', *Phys. Rev. E*, 2003, **67**, 066711, pp. 1–6

34 He, X., and Doolen, G.D.: 'Thermodynamic foundation of kinetic theory and lattice Boltzmann models for multiphase flows', *J. Stat. Phys.*, 2002, **107**, pp. 309–328

35 Nourgaliev, R.R., Dinh, T.N., Theofanous, T.G., and Joseph, D.: 'The lattice Boltzmann equation method: theoretical interpretation, numerics and implications', *Int. J. Multiph. Flow*, 2003, **29**, pp. 117–169

36 Wolfram, S.: 'Cellular automaton fluids 1: basic theory', *J. Stat. Phys.*, 1986, **45**, pp. 471–526

37 Landau, L., and Lifshitz, E.: 'Electrodynamics of continuous media' (Pergamon, New York, 1984)

IET Sci. Meas. Technol., Vol. 1, No. 6, November 2007

311